arXiv:2112.10804v1 [math.NA] 20 Dec 2021

Toward Fast and Provably Accurate Near-field Ptychographic Phase Retrieval

Mark Iwen, Michael Perlmutter, and Mark Philip Roach

December 22, 2021

Abstract

Ptychography is an imaging technique which involves a sample being illuminated by a coherent, localized probe of illumination. When the probe interacts with the sample, the light is diffracted and a diffraction pattern is detected. Then the sample (or probe) is shifted laterally in space to illuminate a new area of the sample whilst ensuring sufficient overlap. Near-field Ptychography (NFP) (see, e.g., [1, 2, 3]) occurs when the sample is placed at a short defocus distance having a large Fresnel number. In this paper, we prove that certain NFP measurements are robustly invertible (up to an unavoidable global phase ambiguity) by constructing a point spread function and physical mask which leads to a well-conditioned lifted linear system. We then apply a block phase retrieval algorithm using weighted angular synchronization and prove that the proposed approach accurately recovers the measured sample. Finally, we also propose using a Wirtinger Flow for NFP problems and numerically evaluate that alternate approach both against our main proposed approach, as well as with NFP measurements for which our main approach does not apply.

1 Introduction

The task of recovering a complex signal $\mathbf{x} \in \mathbb{C}^d$ from phaseless magnitude measurements is called the *phase retrieval problem*. These types of problems appear in many applications such as optics [4, 5] and x-ray crystallography [6, 7]. Here, we are interested in phase retrieval problems arising from ptychography [8], an imaging technique involving a sample illuminated by a coherent and often localized probe of illumination. When the probe interacts with the sample, light is diffracted and a diffraction pattern is detected. The probe, or the sample, is then shifted laterally in space to illuminate a new area of the sample while ensuring there is sufficient overlap between each neighboring shift. The intensity of the diffraction pattern detected at position ℓ resulting from the k^{th} shift of the probe along the sample takes the general form of

$$\tilde{Y}_{k,\ell} = |(D(S_k \mathbf{m} \circ \mathbf{x}))_\ell|^2, \tag{1}$$

where $\mathbf{x} \in \mathbb{C}^d$ is the sample being imaged, $\mathbf{m} \in \mathbb{C}^d$ is a mask which represents the probe's incident illumination on (a portion of) the sample, $\circ$ denotes the Hadamard (pointwise) product, S_k is a shift operator, and $D : \mathbb{C}^d \to \mathbb{C}^d$ is a function that describes the diffraction of the probe radiation from the sample to the plane of the detector after possibly passing though, e.g, a lens.

Prior work in the computational mathematics community related to ptychographic imaging has primarily focused on far-field[1] ptychography (FFP) in which D is the action of a discrete Fourier transform matrix (see, e.g., [10, 11, 12, 13, 14, 15]) in (1). Here, in contrast, we consider the less well studied setting of near-field ptychography (NFP) which describes situations where the masked sample is too close to the detector to be well described by the FFP model. See, e.g., [1, 2, 3] for such imaging applications as well as for more detailed related discussions. In all of these NFP applications the acquired measurements can again be written in the form of (1) where D is now a convolution operator with a given Point Spread Function (PSF) $\mathbf{p} \in \mathbb{C}^d$.

Let $\mathbf{x} \in \mathbb{C}^d$ denote an unknown sample, $\mathbf{m} \in \mathbb{C}^d$ be a known mask, and $\mathbf{p} \in \mathbb{C}^d$ be a known PSF, respectively. For the remainder of this paper we will suppose we have noisy discretized NFP measurements of the form

$$Y_{k,\ell} = Y_{k,\ell}(\mathbf{x}) \coloneqq |(\mathbf{p} * (S_k \mathbf{m} \circ \mathbf{x}))_\ell|^2 + N_{k,\ell}, \quad (k,\ell) \in \mathcal{S} \subseteq [d]_0 \times [d]_0 \tag{2}$$

where S_k is a circular shift operator $(S_k \mathbf{x})_n = \mathbf{x}_{n+k \bmod d}$, $\mathbf{N} = (N_{k,\ell})$ is an additive noise matrix, and $[d]_0 \coloneqq \{0, \dots, d-1\}$. Throughout this paper we will always index vectors and matrices modulo d unless otherwise stated.

1.1 Results, Contributions, and Contents

Our main theorem guarantees the existence of a PSF $\mathbf{p} \in \mathbb{C}^d$ and a locally supported mask $\mathbf{m} \in \mathbb{C}^d$ with $\operatorname{supp}(\mathbf{m}) \subseteq [\delta]_0 \coloneqq \{0, \dots, \delta - 1\}$, $\delta \ll d$, for which the measurements (2) can be inverted up to a global phase factor by a computationally efficient and noise robust algorithm. In particular, we prove the following result which we believe to be the first theoretical error guarantee for a recovery algorithm in the setting of NFP.

Theorem 1 (Inversion of NFP Measurements)**.** *Choose $\delta \in [d]_0$ such that $2\delta - 1$ divides d. One can construct a PSF $\mathbf{p} \in \mathbb{C}^d$ and a mask $\mathbf{m} \in \mathbb{C}^d$ with $\operatorname{supp}(\mathbf{m}) \subseteq [\delta]_0$ such that Algorithm 1 below, when provided with input measurements (2), will return an estimate $\mathbf{x}_{est} \in \mathbb{C}^d$ of $\mathbf{x}$ satisfying*

$$\min_{\phi \in [0, 2\pi)} \|\mathbf{x}_{est} - e^{\mathrm{i}\phi} \mathbf{x}\|_2 \leq C \left(\|\mathbf{x}\|_\infty \frac{d\sqrt{\delta} \sqrt{\|\mathbf{x}_{est}\|_\infty^2 + \|\mathbf{x}_{est}\|_\infty^3}}{|\mathbf{x}_{est}|_{\min}^2} \cdot \|\mathbf{N}\|_{\mathrm{F}} + \sqrt{d\delta \|\mathbf{N}\|_{\mathrm{F}}} \right).$$

Here $C \in \mathbb{R}^+$ is an absolute constant[2], and $|\mathbf{x}_{est}|_{\min}$ denotes the smallest magnitude of any entry in $\mathbf{x}_{est}$.

[1] Far-field versus near-field measurements are defined based on the *Fresnel number* of the imaging system. See, e.g., [9] for details.

Looking at Theorem 1 we can see, e.g., that in the noiseless setting where $\|\mathbf{N}\|_{\mathrm{F}} = 0$ the output $\mathbf{x}_{\mathrm{est}}$ of Algorithm 1 is guaranteed to match the measured signal $\mathbf{x}$ up to a global phase factor whenever $\mathbf{x}_{\mathrm{est}}$ has no zeros.[3] Moreover, the method is also robust to small amounts of additive noise. The proof of Theorem 1 consists of two parts: First, in Section 3, we show that a specific PSF and mask choice results in NFP measurements (2) which are essentially equivalent to far-field ptychographic measurements (4) that are known to be robustly invertible by prior work [11, 12, 14]. This guarantees the existence of a PSF and mask which allow for the robust inversion of (2) up to a global phase. However, these prior works all prove error bounds on $\min_{\phi\in[0,2\pi)} \|\mathbf{x}_{\mathrm{est}} - e^{\mathbb{i}\phi}\mathbf{x}\|_2$ which scale *quadratically* in d (see, e.g., Corollary 3 in [12] and Theorem 1 in [14]). This motivates the second part of the proof in Section 4, where we use the results of [16] to improve these results so that they only depend *linearly* on d. We also note that the improved dependence on d proven in Section 4 for the FFP methods previously analyzed in [11, 12, 14] may be of potential independent interest.

Theorem 1 applies to a specific $\mathbf{p}, \mathbf{m}$ pair (described precisely in Lemma 2). In order to be able to handle more general $\mathbf{p}$ and $\mathbf{m}$, in Section 5, we also show that the NFP measurements (2) may be recovered via a Wirtinger Flow based algorithm, Algorithm 2. This approach is particularly useful in situations where the mask is non-compactly supported and, unlike Algorithm 1, it allows us to use fewer shifts. Similar to Algorithm 1, Algorithm 2 relies on the observation that the NFP measurements (2) are essentially equivalent to FFP measurements as shown in Section 3. In Section 6, we evaluate Algorithms 1 and Algorithm 2, numerically, both individually and in comparison to one another in the case of locally supported masks. Finally, in Section 7, we conclude with a brief discussion of future work.

2 Preliminaries: Prior Results for Far-Field Ptychography using Local Measurements

Our method, described in Algorithm 1, is based on relating the near-field ptychographic measurements (2) to far-field ptychographic measurements of the form

$$\widetilde{Y}_{k,\ell} = \widetilde{Y}_{k,\ell}\left(\mathbf{x}\right) \coloneqq \left|\sum_{n=0}^{d-1} m'_n x_{n+k} e^{-2\pi \mathbb{i} \ell n/d}\right|^2 + N_{k,\ell}, \tag{3}$$

where $\mathbf{m}'$ is a compactly supported mask. If we let $(\check{\mathbf{m}}_\ell)_n \coloneqq \overline{m'_n} e^{-2\pi\mathbb{i}\ell n/d}$, then these measurements can be written as

$$\widetilde{Y}_{k,\ell} = |\langle \check{\mathbf{m}}_\ell, S_k \mathbf{x}\rangle|^2 + N_{k,\ell} \tag{4}$$

[2] In this paper we will use C to denote absolute constants which may change from line to line.

[3] Note that prior work on far-field ptychography assumed that $\mathbf{x}$ itself was non-vanishing (see e.g. [11, 12]). However, requiring $\mathbf{x}_{\mathrm{est}}$ to not vanish is more easily verifiable in practice.

Table 1: Notational Reference Table

Notation	Definition	Notes
$[n]_0$	$[n]_0 = \{0, 1, 2, \ldots, n-1\}$	Zero indexing
$(\mathbf{x})_n$	$\mathbf{x} \in \mathbb{C}^d, (\mathbf{x})_n = x_{n \bmod d}$	Vector circular indexing
$(\mathbf{A})_{i,j}$	$\mathbf{A} \in \mathbb{C}^{m\times n}, (\mathbf{A})_{i,j} = A_{i \bmod m, j \bmod n}$	Matrix circular indexing
$\langle \mathbf{x}, \mathbf{y} \rangle$	$\langle \mathbf{x}, \mathbf{y} \rangle = \sum_{n=0}^{d-1} x_n \overline{y}_n = \mathbf{y}^* \mathbf{x}$	Complex inner product
$\mathrm{supp}(\mathbf{x})$	$\mathrm{supp}(\mathbf{x}) = \{n \in [d]_0 \mid x_n \neq 0\}$	Support
$\mathbf{F}_d$	$(\mathbf{F}_d)_{j,k} = e^{-2\pi \mathbb{i} jk/d}, \forall (j,k) \in [d]_0 \times [d]_0$	Discrete Fourier transform matrix
$\widehat{\mathbf{x}}$	$\widehat{x}_n = (\mathbf{F}_d \mathbf{x})_n = \sum_{k=0}^{d-1} x_k e^{-2\pi \mathbb{i} nk/d}$	Discrete Fourier transform
$\mathbf{F}_d^{-1}\mathbf{x}$	$(\mathbf{F}_d^{-1}\mathbf{x})_n = \frac{1}{d}\sum_{k=0}^{d-1} x_k e^{2\pi \mathbb{i} kn/d}$	Discrete inverse Fourier transform
$S_k(\mathbf{x})$	$(S_k\mathbf{x})_n = x_{(n+k) \bmod d}, \quad \forall n \in [d]_0$	Circular shift
$\widetilde{\mathbf{x}}$	$\widetilde{x}_n = x_{-n \bmod d}, \quad \forall n \in [d]_0$	Reversal
$\mathbf{x} * \mathbf{y}$	$(\mathbf{x} * \mathbf{y})_n = \sum_{k=0}^{d-1} x_k y_{n-k}$	Circular convolution
$\mathbf{x} \circ \mathbf{y}$	$(\mathbf{x} \circ \mathbf{y})_n = x_n y_n$	Hadamard (pointwise) product

where as above S_k denotes a circular shift of length k, i.e., $(S_k\mathbf{x})_n = x_{n+k}$. In [11], phase retrieval measurements of this form are studied when $\mathbf{m}'$ is supported in an interval of length δ for some $\delta \ll d$. The fast phase retrieval (fpr) method used there relies on using a lifted linear system involving a block-circulant matrix to recover a portion of the autocorrelation matrix $\mathbf{x}\mathbf{x}^*$. Specifically, letting $D \coloneqq d(2\delta - 1)$, the authors define a block-circulant matrix $\breve{\mathbf{M}} \in \mathbb{C}^{D\times D}$ by

$$\breve{\mathbf{M}} \coloneqq \begin{pmatrix} \breve{\mathbf{M}}_0 & \breve{\mathbf{M}}_1 & \ldots & \breve{\mathbf{M}}_{\delta-1} & 0 & 0 & \ldots & 0 \\ 0 & \breve{\mathbf{M}}_0 & \breve{\mathbf{M}}_1 & \ldots & \breve{\mathbf{M}}_{\delta-1} & 0 & \ldots & 0 \\ \vdots & \vdots & \vdots & \ddots & \ddots & \vdots & \vdots & \vdots \\ \breve{\mathbf{M}}_1 & \ldots & \breve{\mathbf{M}}_{\delta-1} & 0 & 0 & 0 & \ldots & \breve{\mathbf{M}}_0 \end{pmatrix}. \tag{5}$$

where the matrices $\breve{\mathbf{M}}_k \in \mathbb{C}^{(2\delta-1)\times(2\delta-1)}$ are defined entry-wise by

$$(\breve{\mathbf{M}}_k)_{\ell j} \coloneqq \begin{cases} (\breve{\mathbf{m}}_\ell)_k \overline{(\breve{\mathbf{m}}_\ell)}_{j+k}, & 0 \leq j \leq \delta - k \\ (\breve{\mathbf{m}}_\ell)_k \overline{(\breve{\mathbf{m}}_\ell)}_{j+k-2\delta}, & 2\delta - 1 + k \leq j \leq 2\delta - 2 \text{ and } k < \delta \\ 0, & \text{otherwise.} \end{cases} \tag{6}$$

Letting $\mathbf{z} \in \mathbb{C}^d$ be a vector obtained by subsampling appropriate entries of $\mathrm{vec}(\mathbf{x}\mathbf{x}^*)$, the authors show that, in the noiseless setting,

$$\mathrm{vec}(\widetilde{\mathbf{Y}}) = \breve{\mathbf{M}}\mathbf{z}, \quad \widetilde{\mathbf{Y}} \in \mathbb{C}^{d\times(2\delta-1)}. \tag{7}$$

(See Equation (9) of [11] for explicit details on the arrangement of the entries.) For properly chosen $\mathbf{m}$, the matrix $\breve{\mathbf{M}}$ is invertible, and therefore one may solve

for $\mathbf{z}$ by multiplying by $\widetilde{\mathbf{M}}^{-1}$, i.e., $\mathbf{z} = \widetilde{\mathbf{M}}^{-1}\text{vec}(\mathbf{Y})$. Then, one may reshape $\mathbf{z}$ to recover a $d \times d$ matrix $\widehat{\mathbf{X}}$ whose non-zero entries are estimates of the autocorrelation matrix $\mathbf{x}\mathbf{x}^*$. One may then obtain a vector $\mathbf{x}_{\text{est}}$ which approximates $\mathbf{x}$ by angular synchronization procedure such as the eigenvector-based method which we will discuss in Section 2.1.

In [11], it is shown that exponential masks $\check{\mathbf{m}}_\ell^{(\text{fpr})}$ defined by

$$(\check{\mathbf{m}}_\ell^{(\text{fpr})})_n = \begin{cases} \frac{e^{-(n+1)/a}}{\sqrt[4]{2\delta-1}} \cdot e^{\frac{2\pi i n \ell}{2\delta-1}}, & n \in [\delta]_0 \\ 0, & \text{otherwise} \end{cases}, \quad a \coloneqq \max\left\{4, \frac{\delta-1}{2}\right\} \tag{8}$$

lead to a lifted linear system which is well-conditioned and thus to provable recovery guarantees for the method described above. In particular, we may obtain the following upper bound for the condition number of block-circulant matrix $\widetilde{\mathbf{M}}^{(\text{fpr})}$ obtained when one sets $\check{\mathbf{m}} = \check{\mathbf{m}}_\ell^{(\text{fpr})}$.

Theorem 2 (Theorem 4 and Equation (33) in [11])**.** *The condition number of $\widetilde{\mathbf{M}}^{(fpr)}$, the matrix obtained by setting $\mathbf{m} = \check{\mathbf{m}}_\ell^{(fpr)}$ in (6), may be bounded by*

$$\kappa\left(\widetilde{\mathbf{M}}^{(fpr)}\right) < \max\left\{144e^2, \frac{9e^2(\delta-1)^2}{4}\right\} \leq C\delta^2, \quad C \in \mathbb{R}^+.$$

Furthermore, $\widetilde{\mathbf{M}}^{(fpr)}$ can be inverted in $\mathcal{O}(\delta \cdot d \log d)$-time and its smallest singular value $\sigma_{\min}\left(\widetilde{\mathbf{M}}^{(fpr)}\right)$ is bounded from below by C/δ.

2.1 Angular Synchronization

Inverting $\widetilde{\mathbf{M}}$ as described in the previous subsection allows one to obtain a portion of the autocorrelation matrix $\mathbf{x}\mathbf{x}^*$. This motivates us to consider angular synchronization, the process of recovering a vector $\mathbf{x}$ from (a portion of) its autocorrelation matrix $\mathbf{x}\mathbf{x}^*$ (or an estimate $\widehat{\mathbf{X}}$). One popular approach, which we discuss below, is based on upon first entry-wise normalizing this matrix and then taking the lead eigenvector. Specifically, we define a truncated autocorrelation matrix $\mathbf{X}$ corresponding to the true signal $\mathbf{x}$ by

$$X_{j,k} = \begin{cases} x_j\overline{x_k}, & |j-k| \bmod d < \delta \\ 0, & \text{otherwise.} \end{cases} \tag{9}$$

We also define a truncated autocorrelation matrix $\widehat{\mathbf{X}}$ corresponding to our estimate, $\mathbf{x}_{\text{est}}$, given by

$$\widehat{X}_{j,k} = \begin{cases} (x_{\text{est}})_j\overline{(x_{\text{est}})_k}, & |j-k| \bmod d < \delta \\ 0, & \text{otherwise.} \end{cases} \tag{10}$$

The method from [11] is based upon first solving for $\widehat{\mathbf{X}}$ and then solving for $\mathbf{x}_{\text{est}}$. If $\widehat{\mathbf{X}}$ is a good approximation of $\mathbf{X}$, then the results proved in [17] show that $\mathbf{x}_{\text{est}}$ will be a good approximation of $\mathbf{x}$.

Moving forward, prior works [11, 17] effectively decomposed $\mathbf{X} = \mathbf{X}^{(\theta)} \circ \mathbf{X}^{(\text{mag})}$ into its phase and magnitude matrices by setting $X_{j,k}^{(\text{mag})} = |X_{j,k}|$ and $X_{j,k}^{(\theta)} = X_{j,k}/|X_{j,k}|$ if $|X_{j,k}| \neq 0$ with $X_{j,k}^{(\theta)} = 0$ otherwise. One may then write $\widehat{\mathbf{X}} = \widehat{\mathbf{X}}^{(\theta)} \circ \widehat{\mathbf{X}}^{(\text{mag})}$. Note that by construction, if $\mathbf{x}$ is nonvanishing, then we have $|X_{j,k}^{(\theta)}| = 1$ and $X_{j,k}^{(\text{mag})} > 0$ whenever $|j-k| \bmod d < \delta$. Letting $\mathbf{u} \in \mathbb{C}^d$ be the leading eigenvector of $\widehat{\mathbf{X}}$ and letting $\text{diag}(\widehat{\mathbf{X}}) \in \mathbb{C}^d$ be the main diagonal of $\widehat{\mathbf{X}}$, the output of the resulting algorithm was then $\mathbf{x}_{est} \coloneqq \text{diag}(\widehat{\mathbf{X}}) \circ \mathbf{u}$.

Example 1. *Let $d = 4, \delta = 2$. Then $\widehat{\mathbf{X}}$ defined as in (10) is given by*

$$\widehat{\mathbf{X}} = \begin{pmatrix} |(\mathbf{x}_{est})_0|^2 & (\mathbf{x}_{est})_0\overline{(x_{est})_1} & 0 & (\mathbf{x}_{est})_0\overline{(\mathbf{x}_{est})_3} \\ (\mathbf{x}_{est})_1\overline{(\mathbf{x}_{est})_0} & |(\mathbf{x}_{est})_1|^2 & (\mathbf{x}_{est})_1\overline{(\mathbf{x}_{est})_2} & 0 \\ 0 & (\mathbf{x}_{est})_2\overline{(\mathbf{x}_{est})_1} & |(\mathbf{x}_{est})_2|^2 & (\mathbf{x}_{est})_2\overline{(\mathbf{x}_{est})_3} \\ (\mathbf{x}_{est})_3\overline{(\mathbf{x}_{est})_0} & 0 & (\mathbf{x}_{est})_3\overline{(\mathbf{x}_{est})_2} & |(\mathbf{x}_{est})_3|^2 \end{pmatrix}$$

If we write $(\mathbf{x}_{est})_n = |(\mathbf{x}_{est})_n|e^{\mathrm{i}\theta_n}$, then we may compute

$$\widehat{\mathbf{X}}^{(\theta)} = \begin{pmatrix} 1 & e^{i(\theta_0-\theta_1)} & 0 & e^{i(\theta_0-\theta_3)} \\ e^{i(\theta_1-\theta_0)} & 1 & e^{i(\theta_1-\theta_2)} & 0 \\ 0 & e^{i(\theta_2-\theta_1)} & 1 & e^{i(\theta_2-\theta_3)} \\ e^{i(\theta_3-\theta_0)} & 0 & e^{i(\theta_3-\theta_2)} & 1 \end{pmatrix}$$

One may verify that the lead eigenvector is $\mathbf{u} = (e^{\mathrm{i}\theta_0}\ e^{i\theta_1}\ e^{i\theta_2}\ e^{\mathrm{i}\theta_3})^T$ and therefore

$$\mathbf{x}_{\text{est}} = \sqrt{\text{diag}(\widehat{\mathbf{X}})} \circ \mathbf{u} = (|(\mathbf{x}_{est})_0|e^{\mathrm{i}\theta_0}\ |(\mathbf{x}_{est})_1|e^{\mathrm{i}\theta_1}\ |(\mathbf{x}_{est})_2|e^{\mathrm{i}\theta_2}\ |(\mathbf{x}_{est})_3|e^{\mathrm{i}\theta_3})^T.$$

In Section 4, we will discuss another slightly more sophisticated way for estimating the phases based on Algorithm 3 of [18] which involves taking the smallest eigenvector of an appropriately weighted graph Laplacian. Indeed, this new angular synchronization approach is what ultimately allows for the NFP error bound in Theorem 1 to have improved dependence on signal dimension d over prior FFP error bounds in [11, 12, 14].

3 Near from Far: Guaranteed Near-Field Ptychographic Recovery via Far-Field Results

In this section, we show how to relate the near-field ptychographic measurements (2) to the far-field ptychographic measurements (4). This will allow us to recover $\mathbf{x}$ by using methods similar to those introduced in [11]. In order get nontrivial bounds, we will also need to prove the existence of an admissible PSF and mask

pair, $\mathbf{p} \in \mathbb{C}^d$ and $\mathbf{m} \in \mathbb{C}^d$, which lead to a well conditioned linear system in (7). In particular, we will present a PSF and mask pair such that the resulting block-circulant matrix, denoted $\widetilde{\mathbf{M}}^{(p,m)}$, will have the same condition number as the matrix $\widetilde{\mathbf{M}}^{(\mathrm{fpr})}$ constructed from the masks $\breve{\mathbf{m}}_\ell^{(\mathrm{fpr})}$ defined in (8). Therefore, Theorem 2 will allow us to obtain convergence guarantees for Algorithm 1.

Here, we will set the measurement index set $\mathcal{S}$ considered in (2) to be $\mathcal{S} = \mathcal{K} \times \mathcal{L}$ where $\mathcal{K} = [d]_0$ and $\mathcal{L} = [2\delta - 1]_0$. The following lemma proves that we can rewrite NFP measurements from (2) as local FFP measurements of the form (4) as long as the mask $\mathbf{m}$ has local support and the PSF is periodic. It will be based upon defining masks

$$\breve{\mathbf{m}}_\ell^{(p,m)} \coloneqq \overline{S_\ell \widetilde{\mathbf{p}} \circ \mathbf{m}} \in \mathbb{C}^d, \tag{11}$$

where $\widetilde{\mathbf{p}}$ is the reversal of $\mathbf{p}$ about its first entry modulo d, i.e., $\widetilde{p}_n = p_{-n \bmod d}$ Since the masks $\breve{\mathbf{m}}_\ell^{(p,m)}$ have compact support, this will then yield a lifted set of linear measurements of the type considered in [11, 12, 14].

Lemma 1. *Let $\mathcal{S} = \mathcal{K} \times \mathcal{L} = [d]_0 \times [2\delta - 1]_0$, and recall the measurements*

$$Y_{k,\ell} = |(\mathbf{p} * (S_k \mathbf{m} \circ \mathbf{x}))_\ell|^2, \ (k, \ell) \in \mathcal{S}.$$

defined in (2)*. Suppose that $2\delta - 1$ divides d, that $\mathbf{p} \in \mathbb{C}^d$ is $2\delta - 1$ periodic, and that $\mathbf{m} \in \mathbb{C}^d$ satisfies $\mathrm{supp}(\mathbf{m}) \subseteq [\delta]_0$. Then, we may rearrange the measurements* (2) *into a matrix of FFP-type measurements*

$$\widetilde{Y}_{k,\ell} \coloneqq Y_{-k \bmod d, \ k-\ell \bmod 2\delta-1} = |\langle \breve{\mathbf{m}}_\ell^{(p,m)}, S_k \mathbf{x} \rangle|^2, \ (k, \ell) \in [d]_0 \times [2\delta - 1]_0, \tag{12}$$

where $\breve{\mathbf{m}}_\ell^{(p,m)}$ is defined as in (11)*. As a consequence, recovering $\mathbf{x}$ is equivalent to inverting a block-circulant matrix as described in* (5) – (7)*.*

Proof. By Lemma 9 part 1 , Lemma 8, Lemma 9 part 2, and Lemma 7 from Appendix A, we have that

$$\begin{aligned} Y_{k,\ell} = |(\mathbf{p} * (S_k \mathbf{m} \circ \mathbf{x}))_\ell|^2 &= |\langle S_{-\ell} \widetilde{\mathbf{p}}, \overline{S_k \mathbf{m} \circ \mathbf{x}} \rangle|^2 \\ &= |\langle S_{-\ell} \widetilde{\mathbf{p}} \circ S_k \mathbf{m}, \overline{\mathbf{x}} \rangle|^2 \\ &= |\langle S_k (S_{-\ell-k} \widetilde{\mathbf{p}} \circ \mathbf{m}), \overline{\mathbf{x}} \rangle|^2 \\ &= |\langle S_k (\overline{S_{-\ell-k} \widetilde{\mathbf{p}} \circ \mathbf{m}}), \mathbf{x} \rangle|^2 \\ &= |\langle S_k (\overline{S_{-\ell-k \bmod 2\delta-1} \widetilde{\mathbf{p}} \circ \mathbf{m}}), \mathbf{x} \rangle|^2, \end{aligned}$$

where the last equality uses the fact that $\mathbf{p}$ is $2\delta - 1$ periodic. We may now apply Lemma 9 part 3 to see that

$$Y_{k,\ell} = |\langle S_k (\overline{S_{-\ell-k \bmod 2\delta-1} \widetilde{\mathbf{p}} \circ \mathbf{m}}), \mathbf{x} \rangle|^2 = |\langle (\overline{S_{-\ell-k \bmod 2\delta-1} \widetilde{\mathbf{p}} \circ \mathbf{m}}), S_{-k} \mathbf{x} \rangle|^2.$$

Finally, since $\breve{\mathbf{m}}_\ell^{(p,m)} = \overline{S_\ell \widetilde{\mathbf{p}} \circ \mathbf{m}}$, we see that for all $k \in [d]_0$ and all $\ell \in [2\delta - 1]_0$, we have

$$\widetilde{Y}_{k,\ell} = Y_{-k \bmod d, \ k-\ell \bmod 2\delta-1}$$

$$
\begin{aligned}
&= |\langle(\overline{S_{-(k-\ell)-(-k) \bmod 2\delta-1}\widetilde{\mathbf{p}} \circ \mathbf{m}}), S_{-(-k)}\mathbf{x}\rangle|^2 \\
&= |\langle(\overline{S_{\ell \bmod 2\delta-1}\widetilde{\mathbf{p}} \circ \mathbf{m}}), S_k\mathbf{x}\rangle|^2 \\
&= |\langle \breve{\mathbf{m}}_\ell^{(p,m)}, S_k\mathbf{x}\rangle|^2.
\end{aligned}
$$

□

Remark 1. *If we instead restrict the domain on our NFP measurements to* $(k,\ell) \in \cup_{k\in[d]_0}\{d-k\}\times\{k-2\delta+2,\ldots,k-1,k\} \mod d$ *then we may remove the assumption that* $\mathbf{p}$ *is* $2\delta-1$ *periodic. In particular, if one substitutes* $k = d-k'$ *and* $\ell' = k'-i$ *for some* $0 \le i \le 2\delta-2$*, then one has* $(-k'-\ell') \bmod d = i$*. Thus, since* $0 \le i \le 2\delta-2$*,* $(-\ell'-k') \bmod 2\delta-1 = (-\ell'-k') \bmod d$*, and so we may use the same calculation as above without assuming that* $\mathbf{p}$ *is* $2\delta-1$ *periodic.*

Next, in Lemma 2 below, we will show how to choose a mask $\mathbf{m}$ and PSF $\mathbf{p}$ such that $\breve{\mathbf{m}}_\ell^{(p,m)}$ defined as in (11) and $\breve{\mathbf{m}}^{(\mathrm{fpr})}_{2\ell \bmod 2\delta-1}$ defined as in (8) will only differ by a global phase for each $\ell \in [2\delta-1]_0$. As a consequence, we obtain the desired result that the block-circulant matrix arising from our the NFP measurements (2) is essentially equivalent (up to a row permutation and global phase shift) to the well-conditioned lifted linear measurement operator $\widetilde{\mathbf{M}}^{(\mathrm{fpr})}$ considered in Theorem 2.

Lemma 2. *Let* $\mathbf{p},\mathbf{m} \in \mathbb{C}^d$ *have entries given by*

$$
p_n \coloneqq e^{-\frac{2\pi\mathbb{i}n^2}{2\delta-1}}, \quad \textit{and} \quad m_n \coloneqq \begin{cases} \dfrac{e^{-n+1}/a}{\sqrt[4]{2\delta-1}} \cdot e^{\frac{2\pi\mathbb{i}n^2}{2\delta-1}}, & n \in [\delta]_0 \\ 0, & \textit{otherwise} \end{cases},
$$

where $a \coloneqq \max\left\{4, \dfrac{\delta-1}{2}\right\}$*. Then for all* $\ell \in [2\delta-1]_0$*,* $\breve{\mathbf{m}}_\ell^{(p,m)} = \overline{S_\ell\widetilde{\mathbf{p}} \circ \mathbf{m}}$ *satisfies*

$$
\breve{\mathbf{m}}_\ell^{(p,m)} = e^{\frac{2\pi\mathbb{i}\ell^2}{2\delta-1}} \cdot \breve{\mathbf{m}}^{(fpr)}_{2\ell \bmod 2\delta-1}, \tag{13}
$$

where $\breve{\mathbf{m}}_\ell^{(fpr)}$ *is defined as in* (8)*. As a consequence, if we let* $\widetilde{\mathbf{M}}^{(fpr)}$ *and* $\widetilde{\mathbf{M}}^{(p,m)}$ *be the lifted linear measurement matrices as per* (5) *obtained by setting each* $\breve{\mathbf{m}}_\ell$ *in* (6) *equal to* $\breve{\mathbf{m}}_\ell^{(fpr)}$ *and* $\breve{\mathbf{m}}_\ell^{(p,m)}$*, respectively, then we will have*

$$
\widetilde{\mathbf{M}}^{(p,m)} = \mathbf{P}\widetilde{\mathbf{M}}^{(fpr)} \tag{14}
$$

where $\mathbf{P}$ *is a* $D \times D$ *block diagonal permutation matrix. Thus* $\widetilde{\mathbf{M}}^{p,m}$ *and* $\widetilde{\mathbf{M}}^{fpr}$ *have the same singular values and*

$$
\kappa\left(\widetilde{\mathbf{M}}^{(p,m)}\right) = \kappa\left(\widetilde{\mathbf{M}}^{(fpr)}\right) \le C\delta^2,
$$

where $\kappa(\cdot)$ *denotes the condition number of a matrix.*

Proof. Using the definition of the Hadamard product $\circ$, the circulant shift operator S_ℓ and the reversal operator $\mathbf{x} \mapsto \widetilde{\mathbf{x}}$, we see that

$$(\breve{\mathbf{m}}_\ell^{(p,m)})_n = \overline{(S_\ell \widetilde{\mathbf{p}} \circ \mathbf{m})_n} = \overline{(S_\ell \widetilde{\mathbf{p}})_n \mathbf{m}_n} = \widetilde{\overline{\mathbf{p}}}_{n+\ell} \overline{\mathbf{m}_n} = \overline{\mathbf{p}}_{-n-\ell} \overline{\mathbf{m}_n}.$$

Therefore, inserting the definitions of $\mathbf{p}$ and $\mathbf{m}$ above shows that for $n \in [\delta]_0$

$$\begin{aligned}
(\breve{\mathbf{m}}_\ell^{(p,m)})_n &= e^{\frac{2\pi \mathbb{i}(n+\ell)^2}{2\delta-1}} \cdot \frac{e^{-(n+1)/a}}{\sqrt[4]{2\delta-1}} \cdot e^{-\frac{2\pi \mathbb{i} n^2}{2\delta-1}} \\
&= e^{\frac{2\pi \mathbb{i} n^2}{2\delta-1}} \cdot e^{\frac{4\pi \mathbb{i} n\ell}{2\delta-1}} \cdot e^{\frac{2\pi \mathbb{i} \ell^2}{2\delta-1}} \cdot \frac{e^{-(n+1)/a}}{\sqrt[4]{2\delta-1}} \cdot e^{-\frac{2\pi \mathbb{i} n^2}{2\delta-1}} \\
&= e^{\frac{2\pi \mathbb{i} \ell^2}{2\delta-1}} \left(\frac{e^{-(n+1)/a}}{\sqrt[4]{2\delta-1}} \cdot e^{\frac{2\pi \mathbb{i} n(2\ell)}{2\delta-1}} \right) \;=\; e^{\frac{2\pi \mathbb{i} \ell^2}{2\delta-1}} \left(\breve{\mathbf{m}}^{(\mathrm{fpr})}_{2\ell \bmod 2\delta-1} \right)_n .
\end{aligned}$$

For $n \notin [\delta]_0$, we have $\left(\breve{\mathbf{m}}_\ell^{(p,m)} \right)_n = e^{\frac{2\pi \mathbb{i} \ell^2}{2\delta-1}} \left(\breve{\mathbf{m}}^{(\mathrm{fpr})}_{2\ell \bmod 2\delta-1} \right)_n = 0$. Thus (13) follows.

To prove (14), let $\widetilde{\mathbf{M}}^{(p,m)}$ and $\widetilde{\mathbf{M}}_k^{(p,m)}$ be the matrices obtained by using the mask $\breve{\mathbf{m}}_\ell^{p,m}$ in (5) and (6) and let $\widetilde{\mathbf{M}}^{(\mathrm{fpr})}$ and $\widetilde{\mathbf{M}}_k^{(\mathrm{fpr})}$ be the matrices obtained using $\mathbf{m}_\ell^{(\mathrm{fpr})}$ instead. Then combining (13) and (6) implies that $\left(\widetilde{\mathbf{M}}_k^{(p,m)} \right)_{i,j} = \left(\widetilde{\mathbf{M}}_k^{(\mathrm{fpr})} \right)_{2i \bmod 2\delta-1, j}$. For example, when $j \in [\delta - k + 1]_0$ one may check

$$\begin{aligned}
\left(\widetilde{\mathbf{M}}_k^{(p,m)} \right)_{i,j} &= e^{\frac{2\pi \mathbb{i} i^2}{2\delta-1}} \left(\breve{\mathbf{m}}^{(\mathrm{fpr})}_{2i \bmod 2\delta-1} \right)_k \overline{e^{\frac{2\pi \mathbb{i} i^2}{2\delta-1}} \left(\breve{\mathbf{m}}^{(\mathrm{fpr})}_{2i \bmod 2\delta-1} \right)_{j+k}} \qquad (15) \\
&= \left(\widetilde{\mathbf{M}}_k^{(\mathrm{fpr})} \right)_{2i \bmod 2\delta-1, j},
\end{aligned}$$

and one may perform similar computations in the other cases. Since each $\widetilde{\mathbf{M}}_k^{(p,m)}$ and $\widetilde{\mathbf{M}}_k^{(\mathrm{fpr})}$ have $2\delta-1$ rows and the mapping $i \to 2i$ is a bijection on $\mathbb{Z}/(2\delta-1)\mathbb{Z}$ we see that each $\widetilde{\mathbf{M}}_k^{(p,m)}$ may be obtained by permuting the rows of $\widetilde{\mathbf{M}}_k^{(\mathrm{fpr})}$ (and that the permutation does not depend on k). Therefore, there exists a block diagonal permutation matrix $\mathbf{P}$ such that $\widetilde{\mathbf{M}}^{(p,m)} = \mathbf{P} \widetilde{\mathbf{M}}^{(\mathrm{fpr})}$. Finally, the condition number bound for $\widetilde{\mathbf{M}}^{(p,m)}$ now follows from Theorem 2 and the fact that permuting the rows of a matrix does not change its condition number or any of its singular values. □

Lemma 1 above demonstrates how to recast NFP problems involving locally supported masks and periodic PSFs as particular types of FFP problems. Then, Lemma 2 provides a particular PSF and mask combination for which the resulting FFP problem can be solved by inverting a well-conditioned linear system. Together they imply that, for properly chosen $\mathbf{m}$ and $\mathbf{p}$, one may robustly invert the measurements given in (2) by first recasting the NFP data as modified FFP data and then using the BlockPR approach from [11, 12, 14]. This is the main idea behind Algorithm 1. However, this approach will lead to

theoretical error bounds which scale *quadratically* in d. To remedy this, the final step of Algorithm 1 uses an alternative angular synchronization method (which originally appeared in [18]) based on a weighted graph Laplacian as opposed to previous works which used methods based on, e.g., the methods outlined in Section 2.1. As we shall see in the next section, this will allow us to obtain bounds in Theorem 1 which depend linearly in d rather than quadratically.

Algorithm 1 NFP-BlockPR

Require:

1) Variables $d, \delta, D = d(2\delta - 1)$.
2) A $2\delta - 1$ periodic PSF $\mathbf{p} \in \mathbb{C}^d$, and a mask $\mathbf{m} \in \mathbb{C}^d$ with $\mathrm{supp}(\mathbf{m}) \subseteq [\delta]$.
3) A near-field ptychographic measurement matrix $\mathbf{Y} \in \mathbb{C}^{d \times 2\delta - 1}$.

Ensure: $\mathbf{x}_{\mathrm{est}}$ with $\mathbf{x}_{\mathrm{est}} \approx e^{i\theta}\mathbf{x}$ for some $\theta \in [0, 2\pi]$.

1) Form masks $\breve{\mathbf{m}}_\ell^{(p,m)} = \overline{S_\ell \widetilde{\mathbf{p}} \circ \mathbf{m}}$ and matrices $\widetilde{\mathbf{M}}^{(p,m)}$ as per (5) and (6).
2) Compute $\mathbf{z} = \left(\widetilde{\mathbf{M}}^{(p,m)}\right)^{-1} \mathrm{vec}(\mathbf{Y}) \in \mathbb{C}^D$.
3) Reshape $\mathbf{z}$ to get $\widehat{\mathbf{X}}$ as per Section 2.1 containing estimated entries of $\mathbf{x}\mathbf{x}^*$.
4) Use weighted angular synchronization (Algorithm 3, [18]) to obtain $\mathbf{x}_{\mathrm{est}}$.

4 Error Analysis for Algorithm 1

In this section, we will prove our main result, Theorem 1, which provides accuracy and robustness guarantees for Algorithm 1. For $\mathbf{x} \in \mathbb{C}^d$, we write its n^{th} entry as $x_n =: |x_n| e^{\mathbb{i}\theta_n}$ and let $\mathbf{x}^{(\mathrm{mag})} := (|x_0|, \ldots, |x_{d-1}|)^T$ and $\mathbf{x}^{(\theta)} := (e^{\mathbb{i}\theta_0}, e^{\mathbb{i}\theta_1}, \ldots, e^{\mathbb{i}\theta_{d-1}})^T$ so that we may decompose $\mathbf{x}$ as

$$\mathbf{x} = \mathbf{x}^{(\mathrm{mag})} \circ \mathbf{x}^{(\theta)}. \tag{16}$$

The following lemma upper bounds the total estimation error it terms of its phase and magnitude errors. For a proof, please see Appendix A.

Lemma 3. *Let* $\mathbf{x}$ *be decomposed as in* (16)*, and similarly let* $\mathbf{x}_{est}$ *be decomposed* $\mathbf{x}_{est} = \mathbf{x}_{est}^{(mag)} \circ \mathbf{x}_{est}^{(\theta)}$*. Then, we have that*

$$\min_{\phi \in [0,2\pi)} \left\| \mathbf{x} - e^{\mathbb{i}\phi} \mathbf{x}_{est} \right\|_2 \leq \|\mathbf{x}\|_\infty \min_{\phi \in [0,2\pi)} \left\| \mathbf{x}_{est}^{(\theta)} - e^{\mathbb{i}\phi} \mathbf{x}^{(\theta)} \right\|_2 + \left\| \mathbf{x}^{(mag)} - \mathbf{x}_{est}^{(mag)} \right\|_2. \tag{17}$$

In light of Lemma 3, to bound the total error of our algorithm, it suffices to consider the phase and magnitude errors separately. In order to bound $\|\mathbf{x}^{(\mathrm{mag})} - \mathbf{x}_{\mathrm{est}}^{(\mathrm{mag})}\|_2$, we may utilize the following lemma which is a restatement of Lemma 3 of [11].

Lemma 4 (Lemma 3 of [11])**.** *Let* $\sigma_{\min}\left(\widetilde{\mathbf{M}}^{(p,m)}\right)$ *denote the smallest singular*

value of the lifted measurement matrix $\widetilde{\mathbf{M}}^{(p,m)}$ *from line 1 of Algorithm 1. Then,*

$$\left\|\mathbf{x}^{(mag)} - \mathbf{x}_{est}^{(mag)}\right\|_\infty \leq C\sqrt{\frac{\|\mathbf{N}\|_F}{\sigma_{\min}\left(\widetilde{\mathbf{M}}^{(p,m)}\right)}}.$$

Having obtained Lemma 4, we are now able to prove the following theorem bounding the total estimation error.

Theorem 3. *Let* $\mathbf{p}$ *and* $\mathbf{m}$ *be the admissible PSF, mask pair defined in Lemma 2. Then, we have that*

$$\min_{\phi\in[0,2\pi)} \left\|\mathbf{x} - e^{\mathbb{i}\phi}\mathbf{x}_{est}\right\|_2 \leq \|\mathbf{x}\|_\infty \min_{\phi\in[0,2\pi)} \left\|\mathbf{x}_{est}^{(\theta)} - e^{\mathbb{i}\phi}\mathbf{x}^{(\theta)}\right\|_2 + C\sqrt{d\delta\|\mathbf{N}\|_F}.$$

Proof. Combining Lemmas 3 and 4 along with the inequality $\|\mathbf{u}\|_2 \leq \sqrt{d}\|\mathbf{u}\|_\infty$, implies that

$$\min_{\phi\in[0,2\pi)} \|\mathbf{x} - e^{\mathbb{i}\phi}\mathbf{x}_{\text{est}}\|_2 \leq \|\mathbf{x}\|_\infty \min_{\phi\in[0,2\pi)} \left\|\mathbf{x}_{\text{est}}^{(\theta)} - e^{\mathbb{i}\phi}\mathbf{x}^{(\theta)}\right\|_2 + C\sqrt{\frac{d\|\mathbf{N}\|_F}{\sigma_{\min}\left(\widetilde{\mathbf{M}}^{(p,m)}\right)}}. \tag{18}$$

As noted in Lemma 2, the singular values of $\widetilde{\mathbf{M}}^{(p,m)}$ are the same as those of $\widetilde{\mathbf{M}}^{(\text{fpr})}$. Therefore, applying Theorem 2 then finishes the proof. □

Remark 2. *Note that the inequality* (18) *in the proof of Theorem 3 holds any time* $2\delta-1$ *divides* d, $\mathbf{p} \in \mathbb{C}^d$ *is* $2\delta-1$ *periodic, and* $\mathbf{m} \in \mathbb{C}^d$ *satisfies* $\text{supp}(\mathbf{m}) \subseteq [\delta]_0$. *Therefore, results analogous to Theorem 3 may be produced for any* $\mathbf{p}$ *and* $\mathbf{m}$ *pair such that* $\sigma_{\min}\left(\widetilde{\mathbf{M}}^{(p,m)}\right) > 0$.

In order to bound $\left\|\mathbf{x}_{\text{est}}^{(\theta)} - e^{\mathbb{i}\phi}\mathbf{x}^{(\theta)}\right\|_2$, we will need a few additional definitions. As in (9), let $\mathbf{X}$ denote the partial autocorrelation matrix corresponding to the true signal $\mathbf{x}$ and as in (10), and let $\widehat{\mathbf{X}}$ denote the partial autocorrelation matrix corresponding to $\mathbf{x}_{\text{est}}$, i.e., the matrix obtained in step 3 of Algorithm 1). Let $G = (V, E, \mathbf{W})$ be a weighted graph whose vertices are given by $V = [d]_0$, whose edge set E is taken to be the set of (i, j) such that $i \neq j$ and $|i - j \bmod d| < \delta$, and whose weight matrix $\mathbf{W}$ is defined entrywise by

$$W_{i,j} = \begin{cases} |\widehat{X}_{i,j}|^2, & 0 < |i-j| \bmod d < \delta \\ 0, & \text{otherwise} \end{cases}. \tag{19}$$

Letting $\mathbf{A}_G$ denote the *unweighted* adjacency matrix of G, we observe that by construction, we have $\mathbf{X} = (\mathbf{I}+\mathbf{A}_G)\circ\mathbf{x}\mathbf{x}^*$ and $\widehat{\mathbf{X}} = (\mathbf{I}+\mathbf{A}_G)\circ\mathbf{x}_{\text{est}}\mathbf{x}_{\text{est}}^*$. Letting $\mathbf{D}$ denote the *weighted* degree matrix, we define the *unnormalized graph Laplacian* by $\mathbf{L}_G \coloneqq \mathbf{D}-\mathbf{W}$ and the *normalized graph Laplacian* by $\mathbf{L}_N \coloneqq \mathbf{D}^{-1/2}\mathbf{L}_G\mathbf{D}^{-1/2}$. It is well known that both $\mathbf{L}_G$ and $\mathbf{L}_N$ are positive semi-definite with a minimal

eigenvalue of zero (see, e.g., Section 3.1, [19]). We will let τ_G denote the spectral gap (second smallest eigenvalue) of $\mathbf{L}_G$. It is well known that if G is connected then τ_G is strictly positive (see, e.g., Lemma 3.1.1, [19]).

In [16], the authors used a weighted graph approach to prove the following result which bounds $\min_{\phi\in[0,2\pi)} \|\mathbf{x}_{\text{est}}^{(\theta)} - e^{\mathbb{i}\phi}\mathbf{x}^{(\theta)}\|_2$.

Theorem 4 (Corollary 3, [16])**.** *Consider the weighted graph $G = (V, E, \mathbf{W})$ described in the previous paragraph with weight matrix given as in* (19)*. Let τ_G denote the spectral gap of the associated unnormalized Laplacian $\mathbf{L}_G$. Then we have that*

$$\min_{\phi\in[0,2\pi)} \left\|\mathbf{x}_{est}^{(\theta)} - e^{\mathbb{i}\phi}\mathbf{x}^{(\theta)}\right\|_2 \leq C\sqrt{1+\|\mathbf{x}_{\text{est}}\|_\infty}\cdot\frac{\|\mathbf{X}-\widehat{\mathbf{X}}\|_F}{\sqrt{\tau_G}},\ C\in\mathbb{R}^+.$$

Remark 3. *The $\sqrt{1+\|\mathbf{x}_{est}\|_\infty}$ term is referred to in Theorem 4 of [16] as a tightness penalty which is applied when taking the non-convex constraint and performing an eigenvector relaxation, allowing us to use the method of angular synchronization involving the weighted Laplacian given in Algorithm 3 of [18].*

In order to utilize Theorem 4 we require both an upper bound of $\|\mathbf{X}-\widehat{\mathbf{X}}\|_F$ and a lower bound for the spectral gap τ_G. These are provided by the next two lemmas.

Lemma 5. *Let* $\mathbf{p}$ *and* $\mathbf{m}$ *be defined as in Lemma 2. Then,* $\|\mathbf{X}-\widehat{\mathbf{X}}\|_F \leq C\delta\|\mathbf{N}\|_F$.

Proof. Let $\text{vec}:\mathbb{C}^{d\times d}\to\mathbb{C}^D$ be the vectorization operator considered in (7). It follows from (4), (7), and Step 2 of Algorithm 1, that

$$\text{vec}(\mathbf{Y}) = \widetilde{\mathbf{M}}\text{vec}(\widehat{\mathbf{X}}) \quad \text{and} \quad \text{vec}(\mathbf{Y}-\mathbf{N}) = \widetilde{\mathbf{M}}\text{vec}(\mathbf{X}).$$

Therefore,

$$\left\|\mathbf{X}-\widehat{\mathbf{X}}\right\|_F \leq \left\|\left(\widetilde{\mathbf{M}}^{(p,m)}\right)^{-1}\text{vec}(\mathbf{N})\right\|_2 \leq \frac{\|\text{vec}(\mathbf{N})\|_2}{\sigma_{\min}\left(\widetilde{\mathbf{M}}^{(p,m)}\right)} \leq C\delta\|\mathbf{N}\|_F,$$

where final inequality again utilizes Lemma 2 and Theorem 2. □

Lemma 6. *For the graph G considered in Theorem 4, we have that*

$$\tau_G \geq \frac{|(\mathbf{x}_{est})_{\min}|^4}{\|\mathbf{x}_{est}\|_\infty^2}\frac{4(\delta-1)}{d^2}.$$

Proof. Letting $W_{\min}$ and $W_{\max}$ be the minimum and maximum value of any of the (nonzero) entries of $\mathbf{W}$, we have that $W_{\min}\geq|(\mathbf{x}_{\text{est}})_{\min}^2$, $W_{\max}\leq\|\mathbf{x}_{\text{est}}\|_\infty^2$, and $\text{diam}(G_{\text{unw}})\geq d/(2\delta-1)$ (where $\text{diam}(G_{\text{unw}})$ is the diameter of the unweighted version of G). Therefore, by Theorem 5 in Appendix B, we have that

$$\tau_G \geq \frac{|(\mathbf{x}_{\text{est}})_{\min}|^4}{\|\mathbf{x}_{\text{est}}\|_\infty^2}\frac{2}{(d-1)\text{diam}(G)} \geq \frac{|(\mathbf{x}_{\text{est}})_{\min}|^4}{\|\mathbf{x}_{\text{est}}\|_\infty^2}\frac{4(\delta-1)}{d^2}.$$

□

We shall now finally prove our main result.

The Proof of Theorem 1. By Theorem 3, we have

$$\min_{\phi\in[0,2\pi)} \left\|\mathbf{x} - e^{\mathbb{i}\phi}\mathbf{x}_{\text{est}}\right\|_2 \leq \|\mathbf{x}\|_\infty \min_{\phi\in[0,2\pi)} \left\|\mathbf{x}_{\text{est}}^{(\theta)} - e^{\mathbb{i}\phi}\mathbf{x}^{(\theta)}\right\|_2 + C\sqrt{d\delta\|\mathbf{N}\|_F}.$$

Combining Theorem 4 with Lemmas 5 and 6 yields

$$\begin{aligned}\min_{\phi\in[0,2\pi)} \left\|\mathbf{x}_{\text{est}}^{(\theta)} - e^{\mathbb{i}\theta}\mathbf{x}^{(\theta)}\right\|_2 &\leq C\sqrt{1+\|\mathbf{x}_{\text{est}}\|_\infty}\cdot\frac{\|\mathbf{X}-\widehat{\mathbf{X}}\|_F}{\sqrt{\tau_G}}\\ &\leq C\sqrt{1+\|\mathbf{x}_{\text{est}}\|_\infty}\cdot\frac{d\sqrt{\delta}\|\mathbf{x}_{\text{est}}\|_\infty\|\mathbf{N}\|_F}{|(\mathbf{x}_{\text{est}})_{\min}|^2}.\end{aligned}$$

The result follows. □

5 An Alternate Approach: Near-Field Ptychograhy via Wirtinger Flow

In the previous sections we have demonstrated a particular point spread function and mask for which NFP measurements are guaranteed to allow image reconstruction via Algorithm 1. However, in many real-world scenarios the particular mask and PSF combination considered above are not of the type actually used in practice. For example, in the setting considered in [3] the PSF $\mathbf{p}$ ideally behaves like a low-pass filter (so that, e.g., $\widehat{\mathbf{p}}$ is supported in $\{k\in\mathbb{Z}| -K < k \bmod d < K\}$ for some $K \ll d$), and the mask m is globally supported in $[d]_0$. In contrast, the PSF considered above has its nonzero Discrete Fourier coefficients at frequencies in $\{kd/(2\delta-1)\}_{k\in[2\delta-1]_0}$ (and thus its Fourier support includes large frequencies), and the mask m has small physical support in $[\delta]_0$. This motivates us to we explore a variant of the well known Wirtinger Flow algorithm [20] in this section. This method, Algorithm 2, can be applied to more general set of PSF and mask pairs than Algorithm 1 considered in the previous section.

Suppose we have noiseless NFP measurements of the form

$$Y_{k,\ell} = |(\mathbf{p} * (S_k\mathbf{m}\circ\mathbf{x}))_\ell|^2, \quad (k,\ell)\in\bigcup_{0\leq k\leq K-1}\{d-k\}\times\{K-L+1,\ldots,k\} \bmod d,$$

where $K, L \in [d+1]_0\setminus\{0\}$. Then by the same argument used in Lemma 1 (see also in Remark 1), we can manipulate the measurements above so that we have

$$\widetilde{Y}_{k,\ell} = |\langle\check{\mathbf{m}}_\ell^{(p,m)}, S_k\mathbf{x}\rangle|^2, \quad (k,\ell)\in[K]_0\times[L]_0,$$

where the masks $\check{\mathbf{m}}_\ell^{(p,m)}$ are defined as in (11). We may then reshape these measurements into a vector $\mathbf{y}\in\mathbb{C}^{KL}$ with entries given by

$$y_n := |\langle\check{\mathbf{m}}_{n \bmod L}^{(p,m)}, S_{\lfloor\frac{n}{L}\rfloor}\mathbf{x}\rangle|^2, \quad \forall n\in[KL]_0. \tag{20}$$

After this reformulation, we may then apply a standard Wirtinger Flow Algorithm with spectral initialization. Full details are given below in Algorithm 2.

Algorithm 2 NFP Wirtinger Flow

Require:

1) Size $d \in \mathbb{N}$, number of iterations T, stepsizes $\mu_{\tau+1}$ for $\tau \in [T]_0$.[4]
2) PSF $\mathbf{p} \in \mathbb{C}^d$, mask $\mathbf{m} \in \mathbb{C}^d$, $\breve{\mathbf{m}}_\ell^{(p,m)} = \overline{S_\ell \widetilde{\mathbf{p}} \circ \mathbf{m}}$.
3) Noisy measurements $Y_{k,\ell} = |(\mathbf{p} * (S_k \mathbf{m} \circ \mathbf{x}))_\ell|^2 + N_{k,\ell}$.

Ensure: $\mathbf{x}_{\text{est}} \in \mathbb{C}^d$ with $\mathbf{x}_{\text{est}} \approx e^{i\theta}\mathbf{x}$ for some $\theta \in [0, 2\pi]$

1) Rearrange measurement matrix to form measurement vector $\mathbf{y}$ in (20).
2) Compute $\mathbf{z}_0$ using spectral method (Algorithm 1 in [20]).
3) For $\tau \in [T]_0$, let $\mathbf{z}_{\tau+1} = \mathbf{z}_\tau - \dfrac{\mu_{\tau+1}}{\|\mathbf{z}_0\|^2} \nabla f(\mathbf{z}_\tau)$ where

$$f(\mathbf{z}) \coloneqq \frac{1}{KL} \sum_{n=1}^{KL} \left(\left| \left(S_{-\lfloor \frac{n}{L} \rfloor} \breve{\mathbf{m}}_{n \bmod L}^{(p,m)} \right)^* \mathbf{z} \right|^2 - y_n \right)^2.$$

4) Return $\mathbf{x}_{\text{est}} = \mathbf{z}_T$.

6 Numerical Simulations

In this section, we evaluate Algorithms 1 and 2 with respect to both noise robustness and runtime. Every data point in the plots below reports an average reconstruction error or runtime over 100 tests. For each test, a new sample $\mathbf{x} \in \mathbb{C}^d$ is randomly generated by choosing each entry to have independent and identically distributed (i.i.d.) mean 0 and variance 1 Gaussian real and imaginary parts. We then attempt to recover this sample from the noisy measurements $Y_{k,\ell}(\mathbf{x})$ defined as in (2) where the additive noise matrices $\mathbf{N}$ also have i.i.d. mean 0 Gaussian entries.

In our noise robustness experiments, we plot the reconstruction error as a function of the Signal-to-Noise Ratio (SNR), where we define the reconstruction error by

$$\text{Error}(\mathbf{x}, \mathbf{x}_{\text{est}}) := 10 \log_{10} \left(\frac{\min_\phi \|\mathbf{x} - e^{\mathbf{i}\phi} \mathbf{x}_{\text{est}}\|_2^2}{\|\mathbf{x}\|_2^2} \right),$$

and the SNR by

$$\text{SNR}(\mathbf{Y}, \mathbf{N}) := 10 \log_{10} \left(\frac{\|\mathbf{Y} - \mathbf{N}\|_F}{\|\mathbf{N}\|_F} \right).$$

In these experiments, we re-scale the noise matrix $\mathbf{N}$ in order to achieve each desired SNR level. All simulations were performed using MATLAB R2021b on an Intel desktop with a 2.60GHz i7-10750H CPU and 16GB DDR4 2933MHz memory. All code used to generate the figures below is publicly available at `https://github.com/MarkPhilipRoach/NearFieldPtychography`.

[4] For our numerical simulations in Section 6, we set $\mu_\tau = \min(1 - e^{-\tau/330}, 0.4)$ as suggested in [20].

6.1 Algorithms 1 and 2 for Compactly Supported Masks

In these experiments, we choose the measurement index set for (2) to be $\mathcal{S} = \mathcal{K} \times \mathcal{L}$ where $\mathcal{K} = [d]_0$ and $\mathcal{L} = [2\delta - 1]_0$. As a consequence we see that we consider all shifts $k \in [d]_0$ of the mask while observing only a portion of each resulting noisy near-field diffraction pattern $|\mathbf{p} * (S_k\mathbf{m} \circ \mathbf{x})|^2$ for each k. This corresponds to a physical imaging system where, e.g., the sample and (a smaller) detector are fixed while a localized probe with support size δ scans across the sample. Figure 1 evaluates the robustness and runtime of Algorithm 1 as a function of the SNR and mask support δ in this setting. Looking at Figure 1 one can see that noise robustness increases with the support size of the mask, δ, in exchange for mild increases in runtime.

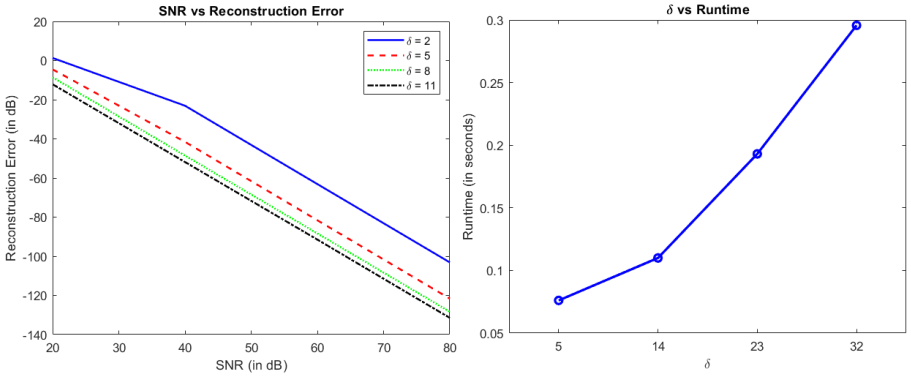


Figure 1: An evaluation of Algorithm 1 for the proposed PSF and mask with $d = 945$. Left: Reconstruction error vs SNR for various $\delta = |\text{supp}(\mathbf{m})|$. Right: Runtime as a function of δ.

Figure 2 compares the performance of Algorithm 1 and Algorithm 2 for the measurements proposed in Lemma 2. Looking at Figure 2 we can see that Algorithm 2 takes longer to achieve comparable errors to Algorithm 1 for these particular $\mathbf{p}$ and $\mathbf{m}$ as SNR increases. More specifically, we see, e.g., that BlockPR achieves a similar reconstruction error to 500 iterations of Wirtinger flow at an SNR of about 50 in a small fraction of the time. This supports the value of the BlockPR method as a fast initializer for more traditional optimization-based solution approaches.

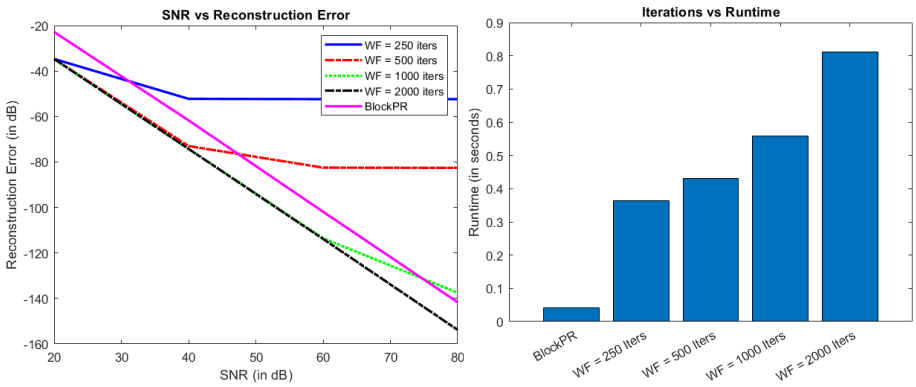


Figure 2: A comparison of Algorithms 1 and 2 for the proposed PSF and mask with $\delta = 26$ and $d = 102$. Left: Reconstruction error vs SNR for various numbers of Algorithm 2 iterations. Right: The corresponding average runtimes.

6.2 Algorithm 2 for Globally Supported Masks

As we saw in the previous section, Algorithm 1 is able to invert NFP measurements more efficiently than Algorithm 2 in situations where it is applicable. However, Algorithm 1 only applies to locally supported masks. In this section, we will show that Algorithm 2 remains effective even when the masks are globally supported, such as the masks considered in [3].

In Figure 3, we evaluate Algorithm 2 using noisy measurements of the form

$$Y_{k,\ell} = |(\mathbf{p} * (S_k \mathbf{m} \circ \mathbf{x}))_\ell|^2 + N_{k,l}, \quad (k,\ell) \in [K]_0 \times [d]_0. \tag{21}$$

Here $\mathbf{p} \in \mathbb{C}^d$ is a low-pass filter with $\widehat{\mathbf{p}} = S_{-(\gamma-1)/2}\mathbb{1}_\gamma$ where $\gamma = \frac{d}{3} + 1$ and $\mathbb{1}_\gamma \in \{0,1\}^d$ is a vector whose first γ entries are 1 and whose last $d-\gamma$ entries are 0. Here, we choose the mask $\mathbf{m}$ to have i.i.d. mean 0 variance 1 Gaussian entries. Thus, the measurements considered in (21) differ from those used in Section 6.1 in two crucial respects: i) the mask $\mathbf{m}$ here has global support. ii) we utilize a small number of mask shifts and observe the entire diffraction pattern resulting from each one (as opposed to observing just a portion of each diffraction pattern from all possible shifts, as above). Examining Figure 3, one can see Algorithm 2 remains effective in this setting. We also observe, as expected, that using more shifts, i.e., collecting more measurements, results in lower reconstruction errors.

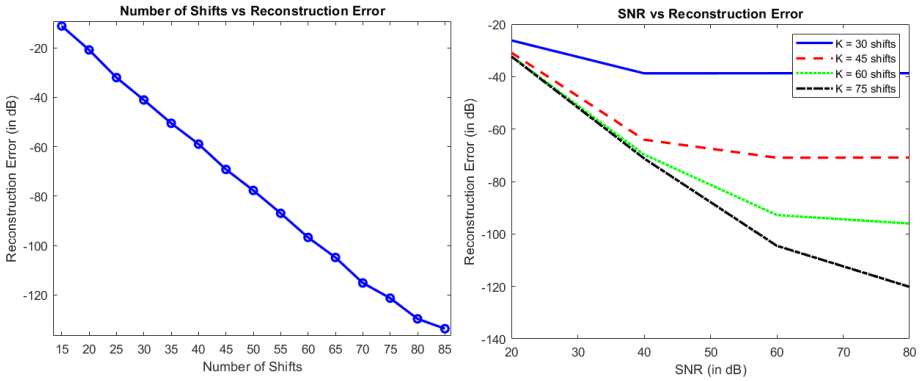


Figure 3: The reconstruction error of Algorithm 2 with $d = 102$, $\mathcal{L} = [d]_0$, and number of iterations $T = 2000$. Left: Reconstruction error vs the number of total shifts K for fixed SNR $= 80$. Right: Reconstruction error vs SNR for various numbers of shifts K.

7 Conclusions and Future Work

We have introduced two new algorithms for recovering a specimen of interest from near-field ptychographic measurements. Both of these algorithms relie on first reformulating and reshaping our measurements so that they resemble widely-studied far-field ptychographic measurements. We then recover our method using either Wirtinger Flow or via methods based on [11]. Algorithm 1 is computational efficient and, to the best of our knowledge, is the first algorithm with provable recovery guarantees for measurements of this form. Algorithm 2, on the other hand, has the advantage of being applied to more general masks with global support. Developing more efficient and provably accurate algorithms for this latter class of measurements remains an interesting avenue for future work.

Acknowledgements

The authors would like to thank Guoan Zheng for answering questions about (and providing code for) his work in [3]. M. Roach's and M. Iwen's work on this project with both supported in part by NSF DMS 1912706.

References

[1] Stockmar, M., Cloetens, P., Zanette, I., Enders, B., Dierolf, M., Pfeiffer, F., Thibault, P.: Near-field ptychography: phase retrieval for inline holography using a structured illumination. Scientific reports **3**(1), 1–6 (2013)

[2] Stockmar, M., Zanette, I., Dierolf, M., Enders, B., Clare, R., Pfeiffer, F., Cloetens, P., Bonnin, A., Thibault, P.: X-ray near-field ptychography for optically thick specimens. Physical Review Applied **3**(1), 014005 (2015)

[3] Zhang, H., Jiang, S., Liao, J., Deng, J., Liu, J., Zhang, Y., Zheng, G.: Near-field fourier ptychography: super-resolution phase retrieval via speckle illumination. Optics express **27**(5), 7498–7512 (2019)

[4] Antonello, J., Verhaegen, M.: Modal-based phase retrieval for adaptive optics. JOSA A **32**(6), 1160–1170 (2015)

[5] Walther, A.: The question of phase retrieval in optics. Optica Acta: International Journal of Optics **10**(1), 41–49 (1963)

[6] Buhler, J., Reichstein, Z.: Symmetric functions and the phase problem in crystallography. Transactions of the American Mathematical Society **357**(6), 2353–2377 (2005)

[7] Liu, Z.-C., Xu, R., Dong, Y.-H.: Phase retrieval in protein crystallography. Acta Crystallographica Section A: Foundations of Crystallography **68**(2), 256–265 (2012)

[8] Rodenburg, J.: Ptychography and related diffractive imaging methods. Advances in Imaging and Electron Physics **150**, 87–184 (2008)

[9] Jenkins, F.A., White, H.E.: Fundamentals of optics. Indian Journal of Physics **25**, 265–266 (1957)

[10] Qian, J., Yang, C., Schirotzek, A., Maia, F., Marchesini, S.: Efficient algorithms for ptychographic phase retrieval. Inverse Problems and Applications, Contemp. Math **615**, 261–280 (2014)

[11] Iwen, M.A., Viswanathan, A., Wang, Y.: Fast Phase Retrieval from Local Correlation Measurements. SIAM Journal on Imaging Sciences **9**(4), 1655–1688 (2016). https://doi.org/10.1137/15m1053761

[12] Iwen, M.A., Preskitt, B., Saab, R., Viswanathan, A.: Phase retrieval from local measurements: improved robustness via eigenvector-based angular synchronization. Applied and Computational Harmonic Analysis **48**, 415–444 (2020)

[13] Fannjiang, A., Zhang, Z.: Fixed point analysis of douglas–rachford splitting for ptychography and phase retrieval. SIAM Journal on Imaging Sciences **13**(2), 609–650 (2020)

[14] Preskitt, B., Saab, R.: Admissible measurements and robust algorithms for ptychography. Journal of Fourier Analysis and Applications **27**(2), 1–39 (2021)

[15] Perlmutter, M., Merhi, S., Viswanathan, A., Iwen, M.: Inverting spectrogram measurements via aliased wigner distribution deconvolution and angular synchronization. Information and Inference: A Journal of the IMA (2020). https://doi.org/10.1093/imaiai/iaaa023

[16] Filbir, F., Krahmer, F., Melnyk, O.: On recovery guarantees for angular synchronization. Journal of Fourier Analysis and Applications **27**(2), 1–26 (2021)

[17] Viswanathan, A., Iwen, M.: Fast angular synchronization for phase retrieval via incomplete information. In: Wavelets and Sparsity XVI, vol. 9597, p. 959718 (2015). International Society for Optics and Photonics

[18] Preskitt, B.P.: Phase Retrieval from Locally Supported Measurements. PhD thesis, University of California, San Diego (2018)

[19] Spielman, D.A.: Spectral and Algebraic Graph Theory. Incomplete Draft, Yale University (2019)

[20] Candes, E.J., Li, X., Soltanolkotabi, M.: Phase retrieval via wirtinger flow: Theory and algorithms. IEEE Transactions on Information Theory **61**(4), 1985–2007 (2015)

A Technical Lemmas

We state the following lemmas for the sake of completeness. Note that we index all vectors modulo d.

Lemma 7. *Let* $\mathbf{x}, \mathbf{y} \in \mathbb{C}^d$. *We have that* $|\langle \mathbf{x}, \overline{\mathbf{y}} \rangle|^2 = |\langle \overline{\mathbf{x}}, \mathbf{y} \rangle|^2$.

Lemma 8. *Let* $\mathbf{x}, \mathbf{y} \in \mathbb{C}^d$. *We have that* $\langle \mathbf{x}, \mathbf{y} \circ \mathbf{z} \rangle = \langle \mathbf{x} \circ \overline{\mathbf{y}}, \mathbf{z} \rangle$.

Proof. By the definition of the inner product and the Hadamard product

$$\langle \mathbf{x}, \mathbf{y} \circ \mathbf{z} \rangle = \sum_{n=0}^{d-1} x_n \overline{(\mathbf{y} \circ \mathbf{z})_n} = \sum_{n=0}^{d-1} x_n \overline{y}_n \overline{z}_n = \sum_{n=0}^{d-1} (\mathbf{x} \circ \overline{\mathbf{y}})_n \overline{z}_n = \langle \mathbf{x} \circ \overline{\mathbf{y}}, \mathbf{z} \rangle.$$

□

Lemma 9. *Let* $\mathbf{x}, \mathbf{y} \in \mathbb{C}^d, k \in \mathbb{Z}$. *We have that*

1. $(\mathbf{x} * \mathbf{y})_k = \langle S_{-k} \widetilde{\mathbf{x}}, \overline{\mathbf{y}} \rangle$;
2. $\mathbf{x} \circ S_k \mathbf{y} = S_k (S_{-k} \mathbf{x} \circ \mathbf{y})$;
3. $\langle S_k \mathbf{x}, \mathbf{y} \rangle = \langle \mathbf{x}, S_{-k} \mathbf{y} \rangle$.

Proof. Proof of 1: Let $\mathbf{x}, \mathbf{y} \in \mathbb{C}^d$. By the definition of the circular convolution

$$(\mathbf{x} * \mathbf{y})_k = \sum_{n=0}^{d-1} x_{k-n} y_n = \sum_{n=0}^{d-1} x_{k-n} \overline{\overline{y_n}} = \sum_{n=0}^{d-1} (S_{-k}\widetilde{\mathbf{x}})_n \overline{\overline{y_n}} = \langle S_{-k}\widetilde{\mathbf{x}}, \overline{\mathbf{y}} \rangle.$$

Proof of 2: Let $\mathbf{x}, \mathbf{y} \in \mathbb{C}^d, k \in \mathbb{Z}$. Let $n \in [d]_0$ be arbitrary. Then we have that

$$(\mathbf{x} \circ S_k \mathbf{y})_n = \mathbf{x}_n (S_k \mathbf{y})_n = (S_{-k}\mathbf{x})_{n+k} \mathbf{y}_{n+k} = (S_k(S_{-k}\mathbf{x} \circ \mathbf{y}))_n.$$

Proof of 3: Noting that we index modulo d, we have that

$$\langle S_k \mathbf{x}, \mathbf{y} \rangle = \sum_{n=0}^{d-1} (S_k \mathbf{x})_n \overline{y_n} = \sum_{n=0}^{d-1} \mathbf{x}_{n+k} \overline{y_n} = \sum_{n=k}^{d+k-1} \mathbf{x}_n \overline{\mathbf{y}_{n-k}} = \sum_{n=0}^{d-1} \mathbf{x}_n \overline{\mathbf{y}_{n-k}} = \langle \mathbf{x}, S_{-k}\mathbf{y} \rangle.$$

□

We now give our proof of Lemma 3.

Proof of Lemma 3. Fix $\phi \in [0, 2\pi)$. By the triangle inequality we have

$$\begin{aligned} \|\mathbf{x} - e^{\mathbb{i}\phi}\mathbf{x}_{\text{est}}\|_2 =& \|\mathbf{x}^{(\text{mag})} \circ \mathbf{x}^{(\theta)} - \mathbf{x}_{\text{est}}^{(\text{mag})} \circ e^{i\phi}\mathbf{x}_{\text{est}}^{(\theta)}\|_2 \\ \leq& \|\mathbf{x}^{(\text{mag})} \circ \mathbf{x}^{(\theta)} - \mathbf{x}^{(\text{mag})} \circ e^{\mathbb{i}\phi}\mathbf{x}_{\text{est}}^{(\theta)}\|_2 \\ &+ \|\mathbf{x}^{(\text{mag})} \circ e^{\mathbb{i}\phi}\mathbf{x}_{\text{est}}^{(\theta)} - \mathbf{x}_{\text{est}}^{(\text{mag})} \circ e^{i\phi}\mathbf{x}_{\text{est}}^{(\theta)}\|_2 \end{aligned} \tag{22}$$

For the first term, we may use the inequality $\|\mathbf{u} \circ \mathbf{v}\|_2 \leq \|\mathbf{u}\|_\infty \|\mathbf{v}\|_2$ to see that

$$\begin{aligned} \|\mathbf{x}^{(\text{mag})} \circ \mathbf{x}^{(\theta)} - \mathbf{x}^{(\text{mag})} \circ e^{\mathbb{i}\phi}\mathbf{x}_{\text{est}}^{(\theta)}\|_2 &\leq \|\mathbf{x}^{(\text{mag})}\|_\infty \|\mathbf{x}_{\text{est}}^{(\theta)} - e^{-\mathbb{i}\phi}\mathbf{x}^{(\theta)}\|_2 \\ &= \|\mathbf{x}\|_\infty \|\mathbf{x}_{\text{est}}^{(\theta)} - e^{-\mathbb{i}\phi}\mathbf{x}^{(\theta)}\|_2. \end{aligned} \tag{23}$$

For the second term, we see that

$$\begin{aligned} \|\mathbf{x}^{(\text{mag})} \circ e^{\mathbb{i}\phi}\mathbf{x}_{\text{est}}^{(\theta)} - \mathbf{x}_{\text{est}}^{(\text{mag})} \circ e^{i\phi}\mathbf{x}_{\text{est}}^{(\theta)}\|_2 &\leq \|e^{\mathbb{i}\phi}\mathbf{x}_{\text{est}}^{(\theta)}\|_\infty \cdot \|\mathbf{x}^{(\text{mag})} - \mathbf{x}_{\text{est}}^{(\text{mag})}\|_2 \\ &= \|\mathbf{x}^{(\text{mag})} - \mathbf{x}_{\text{est}}^{(\text{mag})}\|_2. \end{aligned} \tag{24}$$

Combining (23) and (24) with (22) and minimizing over ϕ completes the proof. □

B Auxilliary Results from Spectral Graph Theory

In this section, we will prove several lemmas related to the graph Laplacian and its eigenvalues. The following definition defines a partial ordering on the set of weighted graphs induced by the spectrum of their graph Laplacians.

Definition 1. *We say that a symmetric matrix* $\mathbf{A}$ *is positive semidefinite and write* $\mathbf{A} \succeq \mathbf{0}$ *if* $\mathbf{x}^T\mathbf{A}\mathbf{x} \geq 0, \forall \mathbf{x} \in \mathbb{R}^n$ *(or equivalently if all the eigenvalues of* $\mathbf{A}$ *are non-negative). We define the Loewner order*[5] $\succeq$ *by the rule that* $\mathbf{A} \succeq \mathbf{B}$ *if* $\mathbf{A} - \mathbf{B}$ *is positive semidefinite (or equivalently if* $\mathbf{x}^T\mathbf{A}\mathbf{x} \geq \mathbf{x}^T\mathbf{B}\mathbf{x}, \forall \mathbf{x} \in \mathbb{R}^n$*). For two graphs* G *and* H *with the same number of vertices, we will define* $G \succeq H$ *if* $\mathbf{L}_G \succeq \mathbf{L}_H$*. We will also write* $G \succeq \sum_{i=0}^{n-1} H_i$ *if* $\mathbf{L}_G \succeq \sum_{i=0}^{n-1} \mathbf{L}_{H_i}$*, and for a scalar* c *we will write* $G \succeq cH$ *if* $\mathbf{L}_G \succeq c\mathbf{L}_H$*.*

Remark 4. *If* $G \succeq H$ *and* τ_G *and* τ_H *are the smallest non-zero eigenvalues* $\mathbf{L}_G$ *and* $\mathbf{L}_H$*, then one can use the fact that* $\tau_G = \min_{\substack{\mathbf{x} \in \mathbb{R}^n \\ \mathbf{x} \perp \mathbf{1}}} \frac{\mathbf{x}^T\mathbf{L}_G\mathbf{x}}{\mathbf{x}^T\mathbf{x}}$ *(see [19]) to verify that* $\tau_G \geq \tau_H$*.*

We now define some basic terminology for weighted graphs. (We note that these definitions may also be applied unweighted graphs by interpreting each edge as having weight one.)

Definition 2. ***(Weighted Distance Definitions)*** *Let* $G = (V, E, \mathbf{W})$ *be a weighted graph.*
(i) For any subgraph $H = (V', E')$ *of* G*, we define the* ***weight*** *of* H*, denoted* $w(H)$*, as*

$$w(H) \coloneqq \sum_{(i,j) \in E'} W_{i,j},$$

(ii) If P *is a path inside* G*, we will let* $len(P) \coloneqq w(P)$ *denote the* ***weighted length*** *of* P*.*
(iii) We define the ***weighted distance*** *between two vertices* u *and* v*,* $dist_G(u, v)$*, to the minimal weighted length of any path from* u *to* v
(iv) The ***weighted diameter*** *of* G*, denoted by* $diam(G)$*, is the maximum distance between any two vertices in* G*, that is,*

$$diam(G) \coloneqq \max\{dist_G(u, v) \mid (u, v) \in V \times V\}$$

In some contexts, it will be useful to consider the pointwise inverses of the weights $W_{i,j}$.

Definition 3. ***(Inverse Weighted Distance Definitions)*** *Let* $G = (V, E, \mathbf{W})$ *be a weighted graph.*
(i) For any subgraph $H = (V', E')$ *of* G*, the* ***inverse weight*** *of* H*, is defined by*

$$w^{-1}(H) \coloneqq \sum_{(i,j) \in E'} \frac{1}{W_{i,j}}$$

[5]The Loewner order is actually a partial ordering since there exist $\mathbf{A}$ and $\mathbf{B}$ such that $\mathbf{A} \not\succeq \mathbf{B}$ and $\mathbf{B} \not\succeq \mathbf{A}$.

*(ii) For a path P inside G, we refer to $len^{-1}(P) \coloneqq w^{-1}(P)$ as the **inverted weighted length** of P.*
*(iii) For two vertices u and v we will refer to the minimal value of $w^{-1}(P)$ over all paths from u to v as the **inverted weighted distance**, denoted by $dist_G^{-1}(u,v)$.*
*(iv) The **inverse weighted diameter** of G, denoted by $diam^{-1}(G)$, is the maximum distance between any two vertices in G, that is,*

$$diam^{-1}(G) \coloneqq \max\{dist_G^{-1}(u,v) \mid (u,v) \in V \times V\}.$$

The proof of Lemma 6 (and thus Theorem 1), relies on the following lemma to provide a lower bound for the spectral gap τ_G.

Lemma 10. *(**Weighted Spectral Bound**) Let $G = (V, E, \mathbf{W})$ be a weighted, connected graph with $|V| = n$, and let $W_{\min}$ and W_{max} denote the minimum and maximum value of any of the (nonzero) weights of G. Then*

$$\tau_G \geq \frac{2 \cdot W_{\min}}{W_{max}(n-1) \cdot diam^{-1}(G)}.$$

To prove Lemma 10, we recall the following lemma from [19].

Lemma 11. ***(Weighted Path Inequality)** (Lemma 5.6.1 [19]) Let $P_n = (v_0, v_1, \ldots, v_{n-1})$ be a path of length n and assume that, for all $0 \leq i < n-2$, w_i, the weight of (v_i, v_{i+1}) is strictly positive. For $0 \leq i < n-2$, let $G_{i,i+1} = (V, (v_i, v_{i+1}))$ be the graph whose vertex set V is that same as the vertex set of G but only has a single edge (v_i, v_{i+1}). Similarly, let $G_{0,n-1} = (V, (v_0, v_{n-1}))$ be the graph with only a single edge (v_0, v_{n-1}). Then*

$$G_{0,n-1} \preccurlyeq \left(\sum_{i=0}^{n-2} \frac{1}{w_i}\right) \sum_{i=0}^{n-2} w_i {G_{i,i+1}}^6 = len^{-1}(P_n) \cdot P_n,$$

where the final equality is interpreted is the sense of $A \preccurlyeq B$ and $B \preccurlyeq A$.

The Proof of Lemma 10. For $u, v \in V$, let $G_{u,v} = (V, (u,v))$ denote the graph with only a single edge from u to v and let $P_{u,v}$ denote a path from u to v with minimal weighted inverse length. Then, by Lemma 11 we have

$$G_{u,v} \preccurlyeq \text{len}^{-1}(P_{u,v}(G)) \cdot P_{u,v}(G) \preccurlyeq \text{diam}^{-1}(G) \cdot P_{u,v}(G) \preccurlyeq \text{diam}^{-1}(G) \cdot G$$

where the last inequality holds since for all subgraphs H of a graph G, $H \preccurlyeq G$ (Section 5.2 [19])

Let $\widetilde{K}_n$ be the extended weighted, complete graph on n vertices with weighted matrix $\widetilde{W}$, where $\widetilde{W}_{i,j} = \begin{cases} W_{i,j}, & (i,j) \in E \\ W_{\min}, & (i,j) \notin E \end{cases}$. Then by summing over all vertices, we have that

$$\mathbf{L}_{\widetilde{K}_n} = \sum_{0 \leq i < j \leq n-1} \widetilde{W}_{i,j} \mathbf{L}_{G_{i,j}} \preccurlyeq W_{\max} \sum_{0 \leq i < j \leq n-1} \text{diam}^{-1}(G) \cdot \mathbf{L}_G$$

[6] Under this construction, we see that if we have a weight which is much larger than all of the others, it effectively gets nullified by taking the inverse.

Since $\sum_{0\leq i<j\leq n-1} 1 = n(n-1)$, we then have that

$$\widetilde{K}_n \preccurlyeq \frac{W_{\max} n(n-1)}{2} \mathrm{diam}^{-1}(G) \cdot G,$$

which, by Remark (4) implies

$$\tau_{\widetilde{K}_n} \leq \frac{W_{\max} n(n-1)}{2} \mathrm{diam}^{-1}(G) \tau_G$$

and therefore

$$\tau_G \geq \frac{2\tau_{\widetilde{K}_n}}{W_{\max} n(n-1) \cdot \mathrm{diam}^{-1}(G)}.$$

Letting K_n be the unweighted graph on n vertices we see that

$$\mathbf{x}^T \mathbf{L}_{\widetilde{K}_n} \mathbf{x} = \sum_{(a,b)\in[n]_0} \widetilde{W}(a,b)(x(a)-x(b))^2 \geq W_{\min} \sum_{(a,b)\in[n]_0} (x(a)-x(b))^2 = W_{\min} \mathbf{x}^T \mathbf{L}_{K_n} \mathbf{x}.$$

Therefore,

$$\tau_{\widetilde{K}_n} = \min_{\substack{\mathbf{x}\in\mathbb{R}^n \\ \mathbf{x}\perp\mathbf{1}}} \frac{\mathbf{x}^T \mathbf{L}_{\widetilde{K}_n} \mathbf{x}}{\mathbf{x}^T \mathbf{x}} \geq W_{\min} \min_{\substack{\mathbf{x}\in\mathbb{R}^n \\ \mathbf{x}\perp\mathbf{1}}} \frac{\mathbf{x}^T \mathbf{L}_{K_n} \mathbf{x}}{\mathbf{x}^T \mathbf{x}} \geq W_{\min} \cdot \tau_{K_n}.$$

Thus, since $\tau_{K_N} = n$ (5.4.1, [19]), we have that $\tau_G \geq \dfrac{2W_{\min}}{W_{\max}(n-1) \cdot \mathrm{diam}^{-1}(G)}$ □

Our next result uses Lemma 10 to produce a bound for τ_G in terms of the diameter of the underlying unweighted graph.

Theorem 5. *Let $G = (V, E, \mathbf{W})$ be a weighted graph and let $W_{\min}$ and W_{max} be the minimum and maximum value of any its (nonzero) weights. Then*

$$\tau_G \geq \frac{2 \cdot (W_{min})^2}{W_{max}(n-1) diam(G_{unw})},$$

where $G_{unw} = (V, E)$ is the unweighted counterpart of G.

Proof. Let $G' = (V, E, \mathbf{W}')$, where $W'_{i,j} = 1/W_{i,j}$ if $W_{i,j} \neq 0$ and $W'_{i,j} = 0$ otherwise. Let $W'_{\max}$ be the maximum element of $\mathbf{W}'$. Observe that by construction, we have $W'_{\max} = \dfrac{1}{W_{\min}}$. Moreover, it follows immediately from Definition 2 that we have $\mathrm{diam}^{-1}(G) = \mathrm{diam}(G')$. Therefore,

$$\mathrm{diam}^{-1}(G) = \mathrm{diam}(G') \leq W'_{\max} \cdot \mathrm{diam}(G_{\mathrm{unw}}) = \frac{1}{W_{\min}} \mathrm{diam}(G_{\mathrm{unw}}).$$

So by Lemma 10, we have that

$$\tau_G \geq \frac{2 \cdot W_{\min}}{W_{\max}(n-1) \cdot \mathrm{diam}^{-1}(G)} \geq \frac{2 \cdot (W_{\min})^2}{W_{\max}(n-1) \mathrm{diam}(G_{\mathrm{unw}})}.$$

□